Oxide ion and proton conductivity in a family of highly oxygen deficient perovskite derivatives

Chloe A. Fuller†, Douglas A. Blom‡, Thomas Vogt††, Ivana Radosavljevic Evans†,*, and John S. O. Evans†,*

† Department of Chemistry, Durham University, Science Site, South Road, Durham DH1 3LE, United Kingdom

‡ Department of Chemical Engineering and NanoCenter, University of South Carolina, Columbia, SC 29208, USA

†† Department of Chemical Engineering, Chemistry and Biochemistry and NanoCenter, University of South Carolina, Columbia, SC 29208, USA

Table S1. Summary of the pellets used, and impedance measurements performed. Ticks in the atmospheres section indicate a dataset was collected under that atmosphere for that sample. Blue shows the data were collected on cooling and red on heating.

Compound	Sintering Conditions / time / h @ temperature / °C	Density / %	Atmospheres	
			Air	Dry N_2
$Ba_3YGa_2O_{7.5}$	24 @ 1200 + 8 @1400	88	✓✓	✓✓
$Ba_{2.95}La_{0.05}YGa_2O_{7.525}$	24 @ 1200 + 8 @ 1400	92	✓	
$Ba_{2.90}La_{0.10}YGa_2O_{7.55}$	24 @ 1200 + 8 @ 1400	92	✓	✓✓
$Ba_3YGa_{1.90}Zn_{0.10}O_{7.45}$	24 @ 1200 + 6 @ 1450	83	✓✓	✓✓
$Ba_3YGa_{1.90}Ti_{0.10}O_{7.55}$	24 @ 1200 + 8 @ 1400	91	✓✓	✓✓
$Ba_3Y_{0.95}Zr_{0.05}Ga_2O_{7.525}$	24 @ 1200 + 8 @ 1400	85	✓✓	✓✓

Table S2. Crystallographic data for the room temperature structure of $Ba_3YGa_2O_{7.5}$ with unit cell parameters a = 7.94820(5) Å, b = 5.96986(4) Å, c = 18.4641(1) Å and β = 91.2927(5)° in space group P2/c.

Atom	Site	*x/a*	*y/b*	*z/c*	Occ.	B_{iso} / Å^2
Ba1	2*e*	0	0.2779(7)	0.25	1	0.83(2)
Ba2	2*f*	0.5	0.3244(6)	0.25	1	0.82(2)
Ba3	4*g*	0.0260(2)	0.7502(6)	0.0895(1)	1	0.76(2)
Ba4	4*g*	0.4994(3)	0.2470(6)	0.5790(1)	1	0.88(2)
Y1	4*g*	0.2468(2)	0.2509(4)	0.4100(1)	1	0.72(2)
Ga1	4*g*	0.24467(19)	0.2536(4)	0.0582(1)	1	0.69(2)
Ga2	4*g*	0.2283(2)	0.7729(3)	0.2662(1)	1	0.66(2)
O1	2*e*	0	0.8010(7)	0.25	1	1.50(6)
O2	4*g*	0.0494(3)	0.7630(5)	0.6095(1)	1	1.15(3)
O3	4*g*	0.4666(3)	0.2460(6)	0.0913(1)	1	1.14(3)
O4	4*g*	0.2761(3)	0.0392(4)	0.3103(1)	1	1.04(4)
O5	4*g*	0.2459(4)	0.5477(4)	0.3360(2)	1	0.94(3)
O6	4*g*	0.2338(4)	0.4895(5)	0.5021(1)	1	0.99(4)
O7	4*g*	0.2309(4)	0.0155(4)	-0.0072(2)	1	0.85(4)
O8	4*g*	0.3107(3)	0.3298(4)	0.6832(1)	1	1.35(4)

Table S3. Bond lengths and angles in the room temperature model of $Ba_3YGa_2O_{7.5}$.

Bond	Bond length / Å		Bond Angle / °						
		Ba1	O2	O2	O4	O4	O1	O5	O5
Ba1—O2	2.6438	O2							
Ba1—O2	2.6438	O2	169.40						
Ba1—O4	2.8242	O4	72.41	102.06					

Ba1—O4	2.8242	O4	119.39	102.06	72.41						
Ba1—O1	2.8470	O1	59.70	59.70	84.70	84.70					
Ba1—O5	2.9657	O5	122.89	64.29	169.10	117.70	68.62				
Ba1—O5	2.9657	O5	114.21	122.89	169.10	64.29	68.62	117.70			
Ba1—O1	3.1228	O1	57.11	57.11	180.00	120.30	120.30	95.30	95.30		
		Ba2	O4	O4	O8	O8	O5	O5	O3		
Ba2—O4	2.7194	O4									
Ba2—O4	2.7194	O4	102.47								
Ba2—O8	2.8219	O8	106.83	128.79							
Ba2—O8	2.8219	O8	85.97	128.79	106.83						
Ba2—O5	2.9193	O5	78.28	62.30	66.17	167.37					
Ba2—O5	2.9193	O5	125.66	62.30	78.28	167.37	66.17				
Ba2—O3	2.9734	O3	124.09	65.37	69.48	125.51	62.78	105.08			
Ba2—O3	2.9734	O3	161.89	65.37	124.09	125.51	69.48	105.08	62.78		
		Ba3	O6	O5	O8	O7	O7	O2	O1	O6	
Ba3—O6	2.7386	O6									
Ba3—O5	2.8563	O5	122.38								
Ba3—O8	2.8575	O8	103.60	77.85							
Ba3—O7	2.8801	O7	160.55	85.67	111.88						
Ba3—O7	2.9120	O7	79.16	90.91	164.84	64.52					
Ba3—O2	2.9349	O2	60.26	68.14	92.42	113.89	123.66				
Ba3—O1	2.9908	O1	77.32	127.19	114.18	59.24	59.72	133.86			
Ba3—O6	3.0642	O6	122.53	127.76	108.49	59.64	139.81	62.81	79.47		
Ba3—O2	3.0910	O2	66.45	89.28	164.36	125.41	125.76	73.58	64.35	61.12	
		Ba4	O8	O5	O7	O6	O3	O3	O6	O7	O3
Ba4—O8	2.5151	O8									
Ba4—O5	2.8143	O5	85.51								
Ba4—O7	2.8967	O7	86.13	154.70							
Ba4—O6	2.9040	O6	123.46	124.15	80.60						
Ba4—O3	2.9638	O3	117.92	68.20	116.95	94.68					
Ba4—O3	3.0468	O3	166.64	58.58	125.00	65.64	72.20				
Ba4—O6	3.0589	O6	65.61	127.69	90.49	59.53	63.33	134.86			
Ba4—O7	3.0643	O7	119.41	119.14	58.03	60.72	91.85	174.97	94.45		
Ba4—O3	3.1621	O3	63.68	55.84	94.90	94.82	65.94	57.54	118.61	145.78	
Ba4—O4	3.1806	O4	125.36	115.67	101.88	122.24	57.75	166.68	68.14	59.30	87.11
		Y1	O7	O6	O5	O4	O3				
Y1—O7	2.2116	O7									
Y1—O6	2.2225	O6	85.85								
Y1—O5	2.2374	O5	87.72	172.83							
Y1—O4	2.2494	O4	86.80	173.60	99.81						
Y1—O3	2.2788	O3	82.08	89.61	94.59	94.06					
Y1—O2	2.3750	O2	170.28	88.68	86.88	94.32	90.45				
		Ga1	O2	O6	O3						
Ga1—O2	1.8391	O2									
Ga1—O6	1.8516	O6	107.67								
Ga1—O3	1.8543	O3	103.69	129.53							

Ga1—O7	1.8667	O7	103.65	105.52	104.73
		Ga2	O8	O4	O1
Ga2—O8	1.7885	O8			
Ga2—O4	1.8223	O4	127.25		
Ga2—O1	1.8401	O1	100.84	105.71	
Ga2—O5	1.8654	O5	103.67	107.96	108.77

Table S4. Crystallographic data for the high-temperature structure of $Ba_3YGa_2O_{7.5}$ with unit cell parameters a = 12.0602(1) Å, b = 9.8282(2) Å, c = 8.04982(6) Å and γ = 107.844(3)° at 1000 °C in space group $P112_1/a$.

Atom	Site	*x/a*	*y/b*	*z/c*	Occ.	B_{iso} / Å^2
Ba12-1	4*e*	0.2721(3)	0.0036(5)	0.0022(8)	1	3.88(9)
Ba34-1	4*e*	0.0884(4)	0.3323(4)	0.4917(5)	1	2.58(7)
Ba34-2	4*e*	0.0860(4)	0.3266(4)	0.0188(5)	1	3.09(9)
Y1	4*e*	0.3342(6)	0.3229(3)	0.7464(6)	1	1.74(5)
Ga1	4*e*	0.3418(5)	0.3848(2)	0.2528(6)	1	1.76(5)
Ga2	4*e*	0.0041(6)	0.0360(3)	0.7802(4)	1	1.66(7)
O1	2*a*	0	0	0	1	7.9(3)
O23-1	4*e*	0.3248(8)	0.2985(7)	0.4595(8)	1	3.25(16)
O23-2	4*e*	0.3165(9)	0.2986(8)	0.0437(9)	1	3.98(19)
O45-1	4*e*	0.1650(6)	0.1385(6)	0.7618(9)	1	2.80(13)
O45-2	4*e*	0.4233(7)	0.1684(7)	0.7492(10)	1	3.34(15)
O6	4*e*	0.5030(6)	0.5002(7)	0.2539(9)	1	1.78(11)
O7	4*e*	0.2548(10)	0.5087(9)	0.2637(12)	1	4.8(2)
O8	4*e*	0.0081(10)	0.1303(9)	0.3199(8)	1	9.9(4)

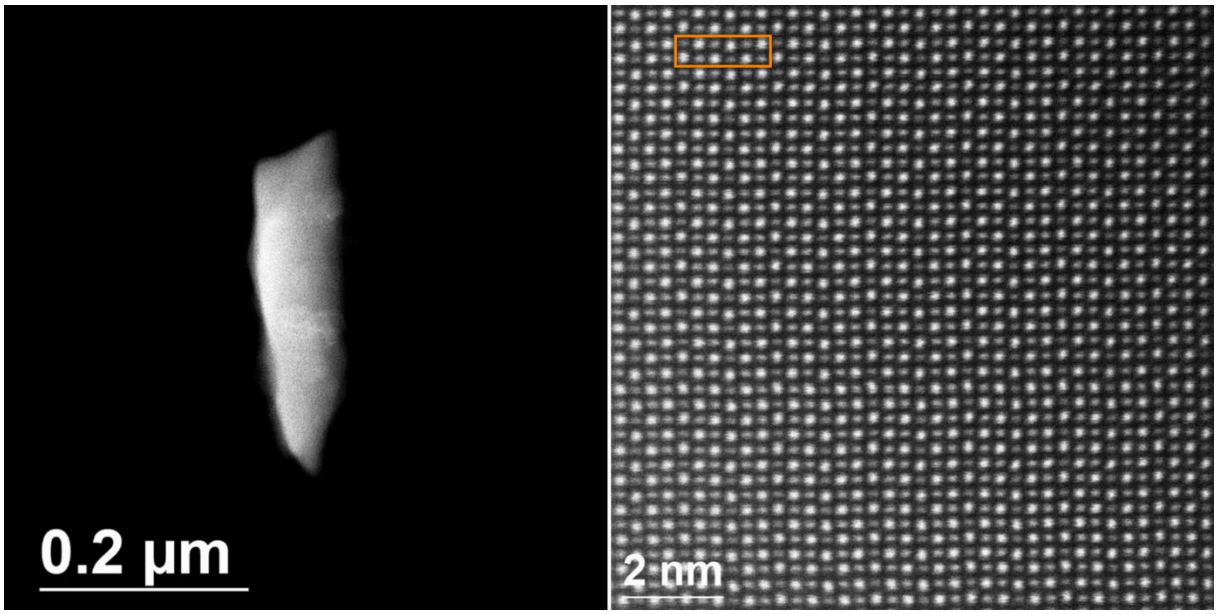

Figure S1. HAADF STEM images of a crystallite of $Ba_3YGa_2O_{7.5}$ (left) and a magnified portion of it (right), containing approximately 106 unit cells.

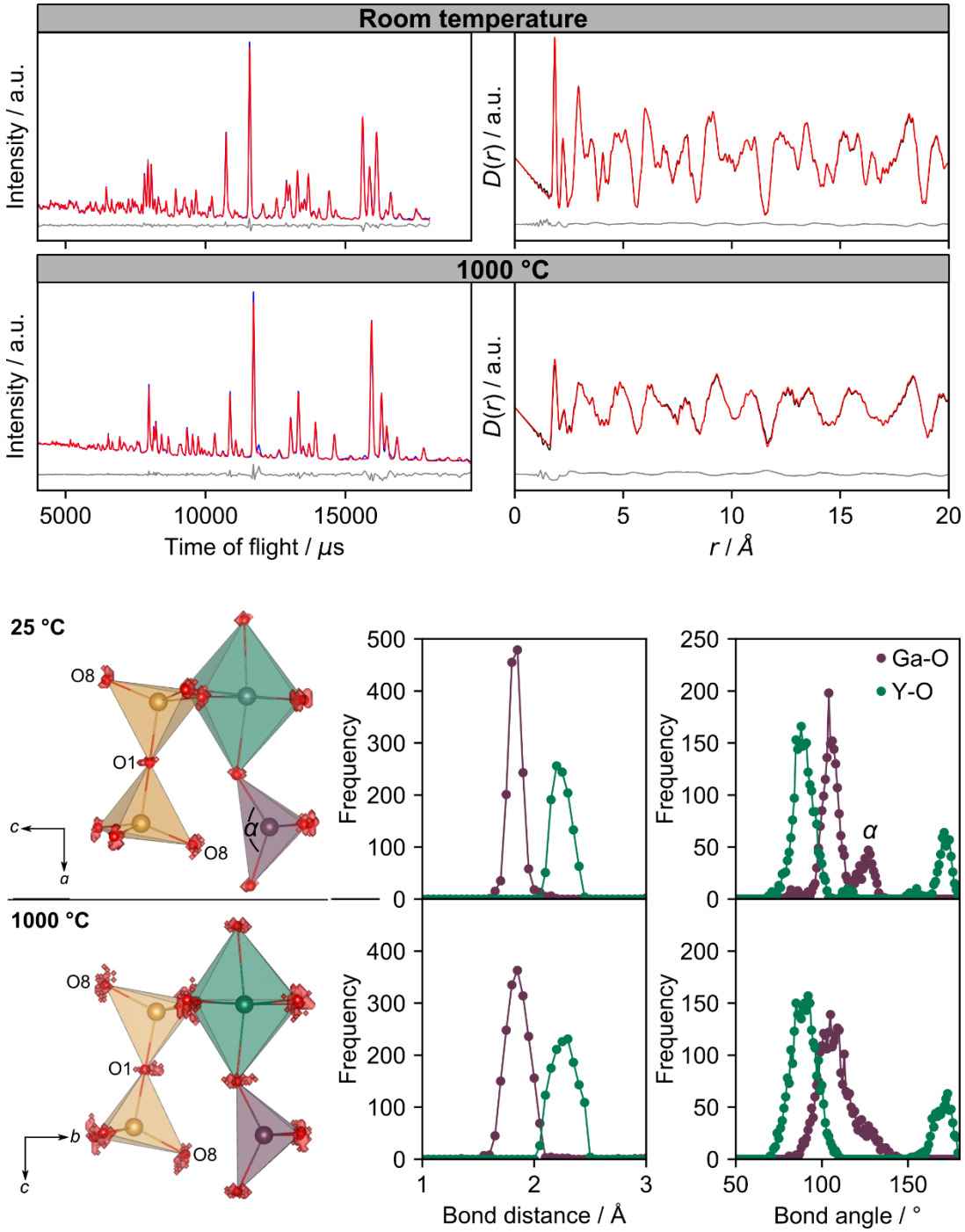

Figure S2. Upper panels show fits to the Bragg and PDF data for $Ba_3YGa_2O_{7.5}$ at 25 °C (R_{wp} = 3.70%) and 1000 °C (R_{wp} = 3.32%). Lower panels show cloud plots illustrating the distribution of oxygen positions at 25 °C and 1000 °C and the distribution of bond distances and angles within metal-centred polyhedral in each model. For 25 °C PDF fitting, the monoclinic P2/c model derived from the joint X-ray and neutron refinement was used to create an approximately isotropic 4×6×2 supercell containing 2592 atoms, and the model was refined simultaneously against the neutron Bragg and the PDF data, subject to local restraints to keep sensible geometries for coordination polyhedra. Oxygen cloud plots (shown in red in the lower left panels) were obtained by folding the PDF-fit supercell into a single average unit cell and are shown superimposed on the Rietveld-derived atomic positions. An equivalent procedure was followed for the 1000 °C data based on the Tamazyan model of Table S2. At both temperatures, the oxygen clouds are centred on the Rietveld-derived oxygen positions. The spread of positions required to fit the data rises at high temperature, consistent with increased thermal motion. The distribution of positions around O1 and O8 sites is consistent with slightly larger displacements of these oxygens, but we do not see the high level of disorder that would be associated with a Cmcm orthorhombic structure.

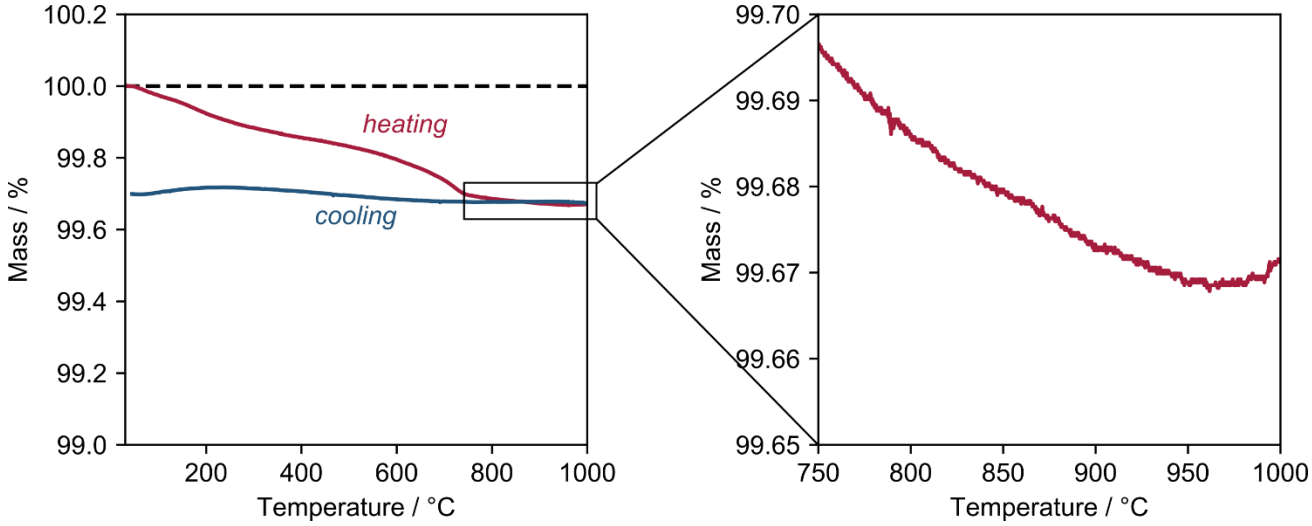

Figure S3. TGA trace of a sample of $Ba_3YGa_2O_{7.5}$ in dry air following heating at 1150 °C for 8.5 h and cooling to 150 °C at 5 K min^{-1}.

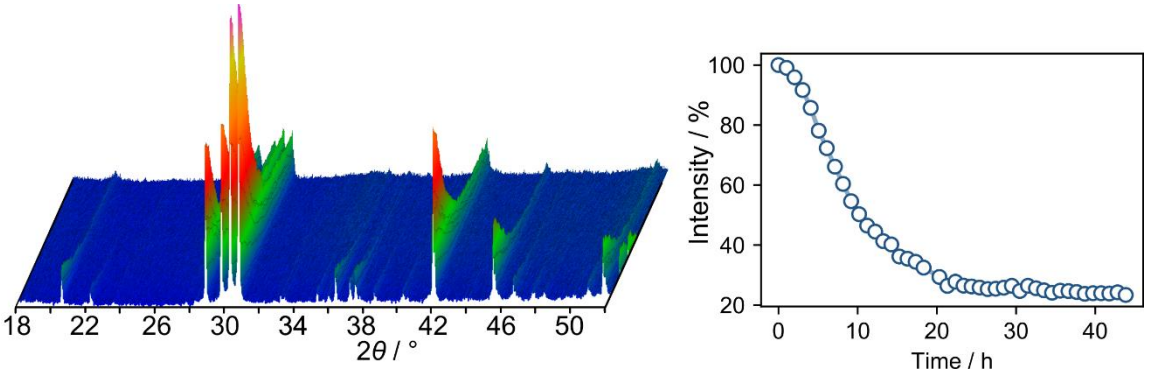

Figure S4. Diffraction patterns, left, and relative intensities of the main reflections, right, of dried $Ba_3YGa_2O_{7.5}$ as a function of time. Each pattern was measured for 1 h.

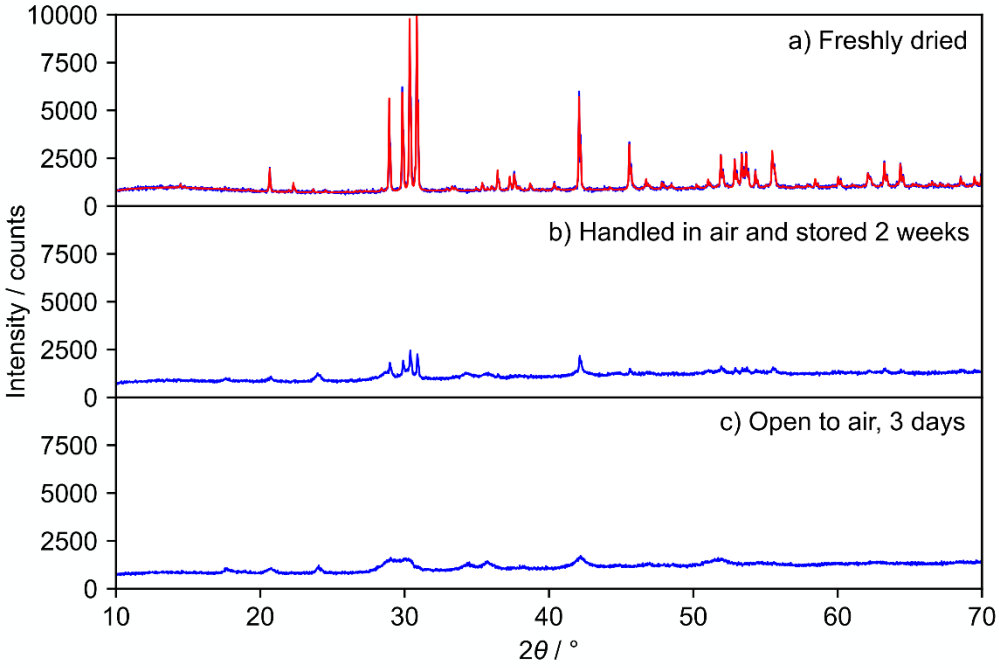

Figure S5. PXRD patterns of $Ba_3YGa_2O_{7.5}$ samples with different thermal histories. The y-scale is the same for all three panels to emphasise the differences. a) The freshly dried sample was heated at 1200 °C for 12 h and quench cooled. b) Sample slow cooled, handled in air and stored without special precautions for 2 weeks. c) Sample was stored in a glass vial with no lid. All three samples originated from the same batch. If samples such as that in c) are heated to ~900 °C (Figure S8), rapid recrystallization occurs to give a diffraction pattern comparable to that in part a), with equally sharp peaks after heating to 1200 °C.

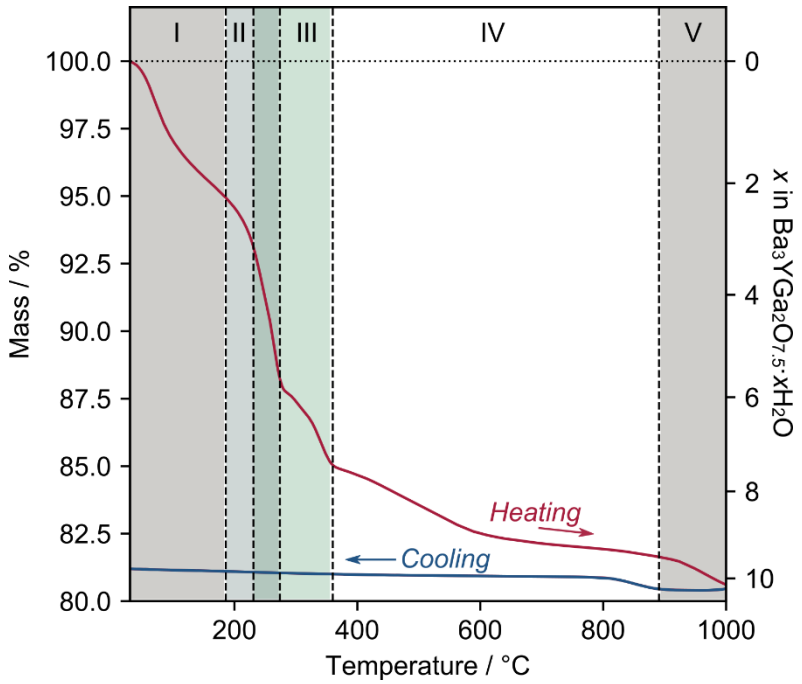

Figure S6. TGA trace of $Ba_3YGa_2O_{7.5}$ after full hydration on heating and subsequent cooling in air. Dotted vertical lines indicate the temperatures at which transitions are observed in the corresponding PXRD experiment of Figure S8; shaded boxes and Roman numerals show which phase is present in each temperature region of Figure S8. $Ba_{2.9}La_{0.1}YGa_2O_{7.55}$ and $Ba_3YGa_{1.9}Zn_{0.1}O_{7.45}$ showed similar behavior.

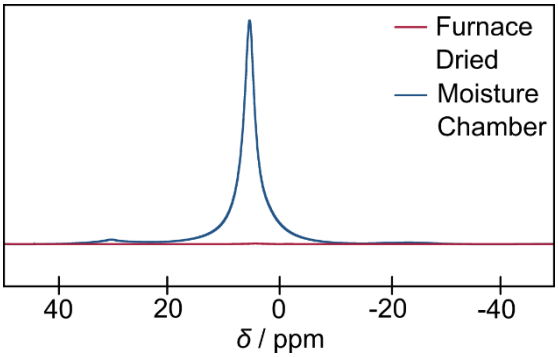

Figure S7. Proton NMR spectra of $Ba_3YGa_2O_{7.5}$ immediately after heating at 1200 °C, and after holding in a 74% moisture chamber for 1 week.

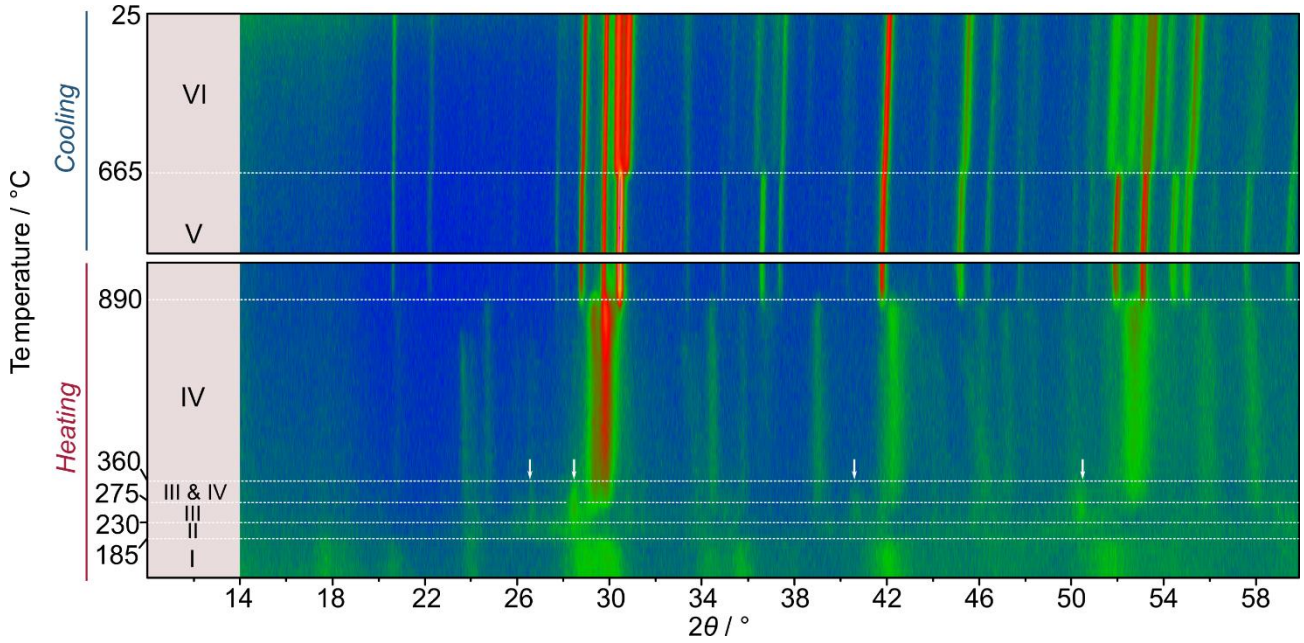

Figure S8. Evolution of the PXRD patterns of hydrated $Ba_3YGa_2O_{7.5}$ on heating and cooling. The temperature scale for the heating panel has been expanded to show the low temperature region more clearly. Dashed lines indicate phase transitions, and the corresponding temperatures are marked. Roman numerals are used to denote the different intensity patterns in each region where each pattern likely corresponds to different set of phases. White arrows highlight the peaks belonging to pattern/phase III as this only exists over a small temperature range and is easily overlooked.

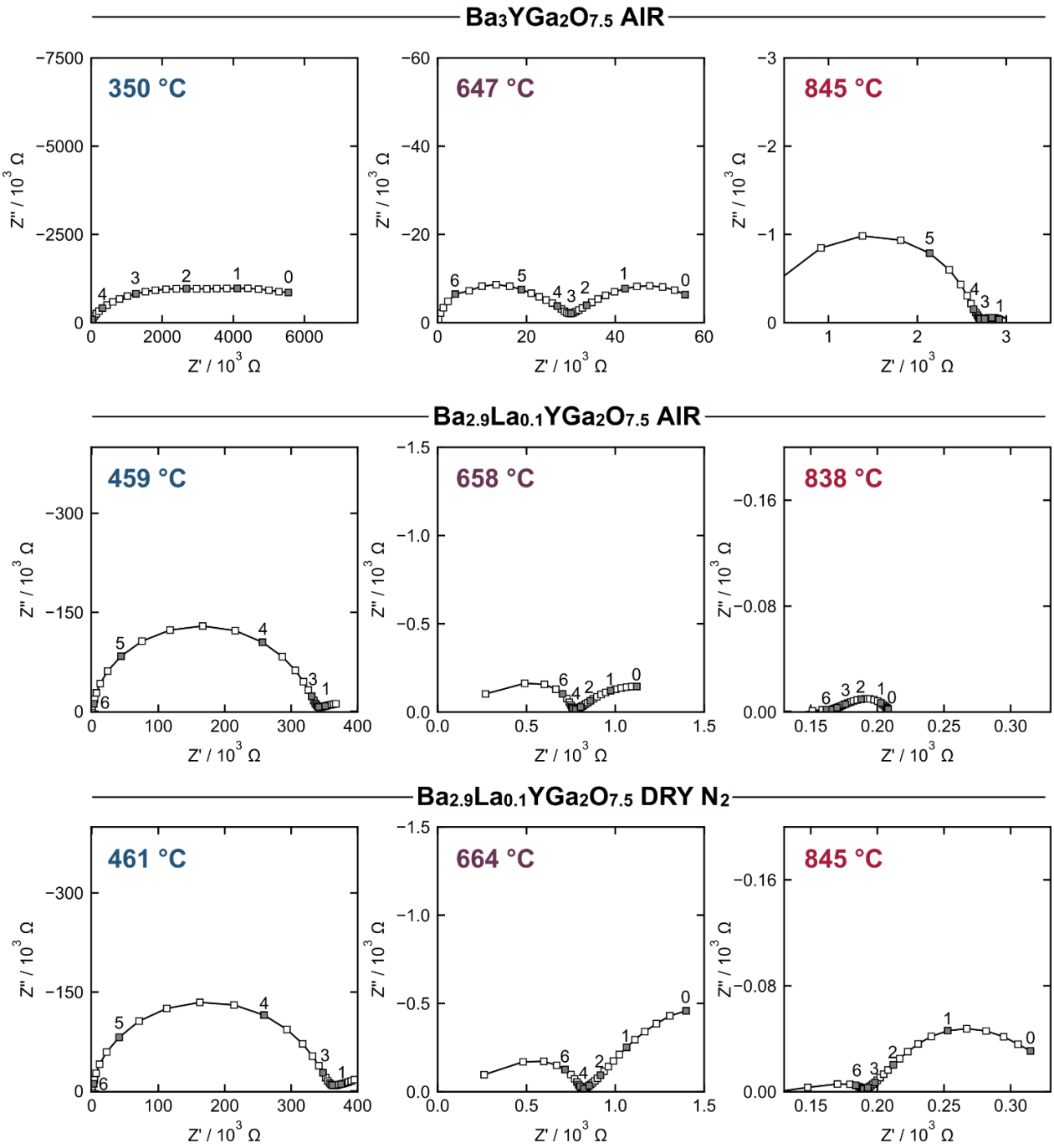

Figure S9. Example complex plane impedance spectra at low, mid and high temperature for $Ba_3YGa_2O_{7.5}$ and $Ba_{2.9}La_{0.1}YGa_2O_{7.5}$. Filled grey squares mark specific frequencies, and the number above it shows the frequency logarithm. The shape of the complex impedance plots for both compounds change significantly with temperature, particularly at the phase transition. For $Ba_3YGa_2O_{7.5}$, there is no obvious semi-circular signal at low temperatures, with the various sample responses overlapping to create a horizontal line. In $Ba_{2.9}La_{0.1}YGa_2O_{7.55}$, by 400 °C the expected semicircle has formed, corresponding to a capacitance of ~10^{-12} F cm^{-1} (from $\omega RC = 1$ at the arc maximum) representing bulk transport. At intermediate temperatures, two distinct signals can be resolved for both compounds, and the capacitances of the high- and low-frequency semicircles were ~10^{-12} and 10^{-6}-10^{-5} F cm^{-1}, respectively, corresponding to bulk transport and a surface layer or electrode response. For $Ba_{2.9}La_{0.1}YGa_2O_{7.55}$, the low frequency response is characteristic of a Warburg-type electrode response, exemplified by the linear incline at approximately 45°, (particularly in the measurements under dry nitrogen). This behaviour is indicative of ionic conductivity with oxide ions able to diffuse into the electrode, and the prevalence of the Warburg response in $Ba_{2.9}La_{0.1}YGa_2O_{7.55}$ relative to $Ba_3YGa_2O_{7.5}$ is consistent with the increase in conductivity. At high temperatures, both semicircles remain in $Ba_3YGa_2O_{7.5}$ with the bulk signal becoming larger relative to the lower frequency signal. In contrast, the bulk signal in $Ba_{2.9}La_{0.1}YGa_2O_{7.55}$ is no longer present leaving only the signal from the electrode response which turns over to form a semicircle. The disappearance of the bulk semicircle is often seen in highly conductive samples at high temperatures when using this experimental setup, and the change in electrode behaviour indicates the ionic diffusion now occurs across the full thickness of the electrode.[1]

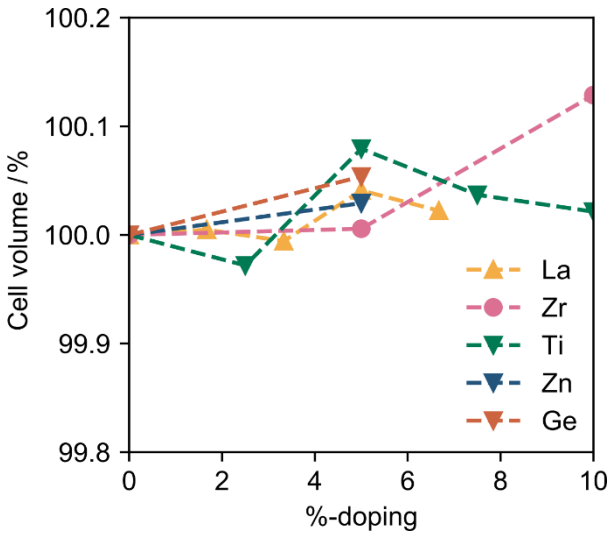

Figure S10. Cell volumes of substituted samples of $Ba_3YGa_2O_{7.5}$. Upwards triangles, circles and downward triangles indicate substitution on the A, Oh and Td sites respectively. Substituent concentration is expressed as the percentage of atoms replaced on a particular site.

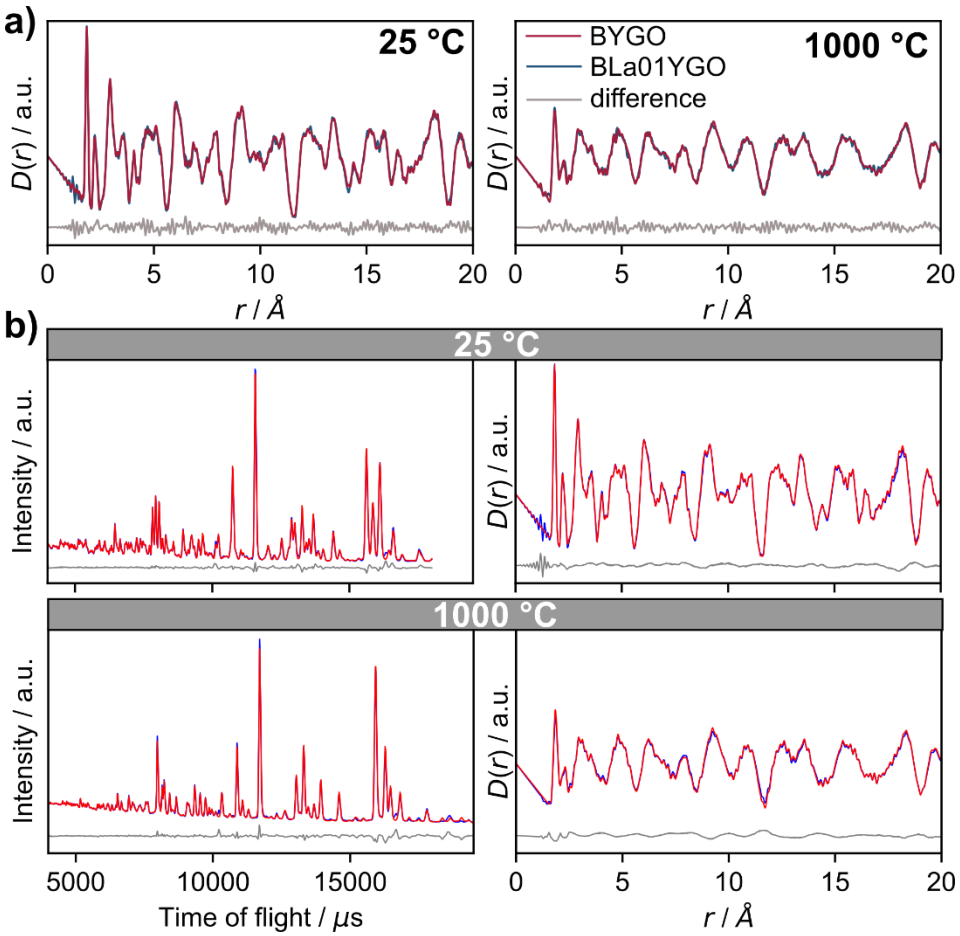

Figure S11. a) Superposition of the raw D(r) data for $Ba_3YGa_2O_{7.5}$ and $Ba_{2.9}La_{0.1}YGa_2O_{7.55}$ measured on POLARIS at both 25 °C and 1000 °C; differences are minor at both temperatures. b) Fits of P2/c (25 °C) and Tamazyan models (1000 °C) with added oxygen interstitials to the Bragg and PDF data of $Ba_{2.9}La_{0.1}YGa_2O_{7.55}$. R_{wp} (25 °C) = 3.34%, R_{wp} (1000 °C) = 2.23%.

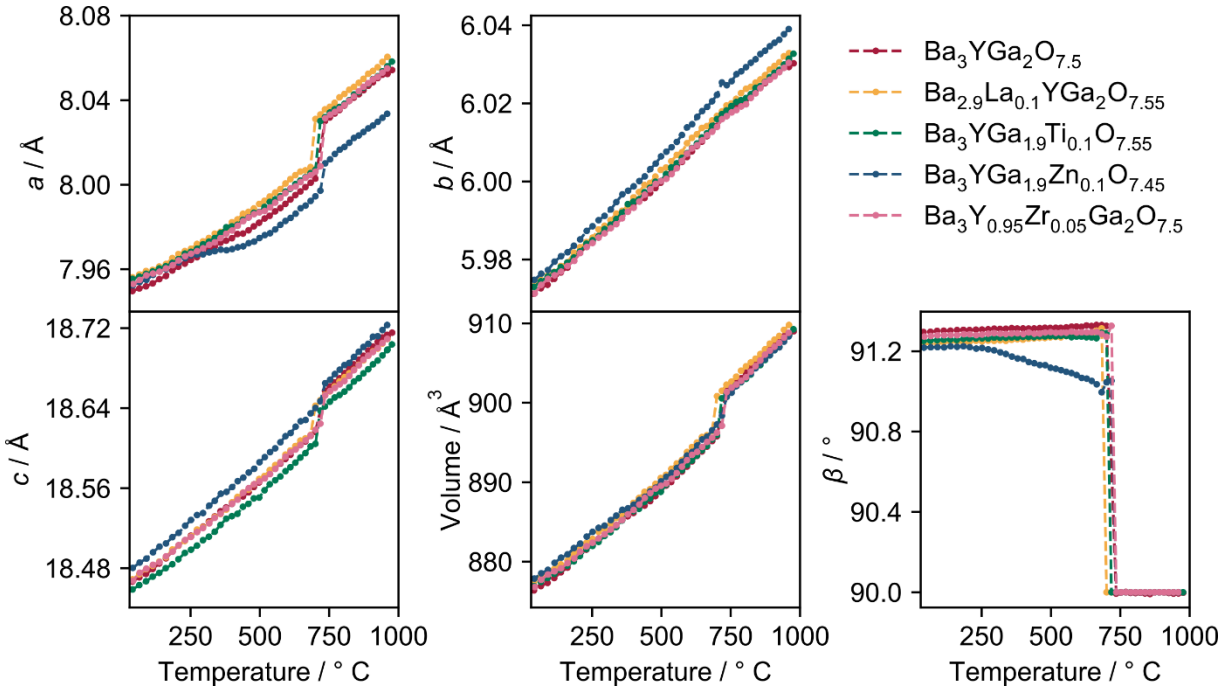

Figure S12. Evolution of the unit-cell parameters with temperature of various substituted $A_3OhTd_2O_{7.5}$ compounds. All values presented here are from cooling cycles but there were no significant differences between heating and cooling.

References

1. Irvine, J.T.S.; Sinclair, D.C.; West, A.R., Electroceramics: Characterization by Impedance Spectroscopy. *Advanced Materials* **1990**, 2(3), 132